

Evaluating physical changes of iron oxide nanoparticles due to surface modification with oleic acid

S Rosales, N Casillas, A Topete, O Cervantes, G González, J A Paz, M E Cano

Citation: Chin. Phys. B . 2020, 29(10): 100502 . **doi:** 10.1088/1674-1056/aba2dc
Journal homepage: http://cpb.iphy.ac.cn; http://iopscience.iop.org/cpb

What follows is a list of articles you may be interested in

Fast and accurate determination of phase transition temperature via individual generalized canonical ensemble simulation

Ming-Zhe Shao(邵明哲), Yan-Ting Wang(王延颋), Xin Zhou(周昕)

Chin. Phys. B . 2020, 29(8): 080505 . **doi:** 10.1088/1674-1056/ab9c03

Effect of transversal concentration gradient on H_2-O_2 cellular detonation

Cheng Wang(王成), Yi-Xuan Wu(吴易烜), Jin Huang(黄金), Wen-Hu Han(韩文虎), Qing-Guan Song(宋清官)

Chin. Phys. B . 2020, 29(6): 060503 . **doi:** 10.1088/1674-1056/ab81f5

Fluctuation theorem for entropy production at strong coupling

Y Y Xu(徐酉阳), J Liu(刘娟), M Feng(冯芒)

Chin. Phys. B . 2020, 29(1): 010501 . **doi:** 10.1088/1674-1056/ab592d

The heat and work of quantum thermodynamic processes with quantum coherence

Shanhe Su(苏山河), Jinfu Chen(陈劲夫), Yuhan Ma(马宇翰), Jincan Chen(陈金灿), Changpu Sun(孙昌璞)

Chin. Phys. B . 2018, 27(6): 060502 . **doi:** 10.1088/1674-1056/27/6/060502

Three-dimensional flow of Powell-Eyring nanofluid with heat and mass flux boundary conditions

Tasawar Hayat, Ikram Ullah, Taseer Muhammad, Ahmed Alsaedi, Sabir Ali Shehzad

Chin. Phys. B . 2016, 25(7): 074701 . **doi:** 10.1088/1674-1056/25/7/074701

Evaluating physical changes of iron oxide nanoparticles due to surface modification with oleic acid

S Rosales[1], N Casillas[1], A Topete[3], O Cervantes[1], G González[1], J A Paz[2], and M E Cano[2,†]

[1] *Centro Universitario de Ciencias Exactas e Ingenierías, Universidad de Guadalajara, Blvd. Marcelino García Barragán* 1421, *C. P.* 44430, *Guadalajara, Jalisco, México*

[2] *Centro Universitario de la Ciénega, Universidad de Guadalajara, Av. Universidad* 1115, *C. P.* 47820, *Ocotlán, Jalisco, México*

[3] *Centro Universitario de Ciencias de la Salud, Universidad de Guadalajara, Sierra Mojada* 950, *C. P.* 44340, *Guadalajara, Jalisco, México*

(Received 1 February 2020; revised manuscript received 13 June 2020; accepted manuscript online 6 July 2020)

The physical characterization of a colloidal system of superficially modified magnetic nanoparticles (MNPs) is presented. The system consists of oleic acid-coated iron oxide nanoparticles (OAMNP) suspended in water. A structural analysis is carried out by using standard physical techniques to determine the diameter and shape of the MNPs and also the width of the coating shell. The colloidal stability and the polydispersity index of this ferrofluid are determined by using Zeta potential measurements. Additionally, the magnetic characterization is conducted by obtaining the DC magnetization loops, and the blocking temperatures are determined according to the ZFC–FC protocol. Finally, the values of power absorption density P of the ferrofluid are estimated by using a magneto-calorimetric procedure in a wide range of magnetic field amplitude H and frequency f. The experimental results exhibit spherical-like shape of OAMNP with (20 ± 4) nm in diameter. Due to the use of coating process, the parameters of the magnetization loops and the blocking temperatures are significantly modified. Hence, while the uncoated MNPs show a blocking state of the magnetization, the OAMNP are superparamagnetic above room temperature (300 K). Furthermore, the reached dependence P *versus* f and P *versus* H of the ferrofluid with coated MNPs are clearly fitted to linear and quadratic correlations, respectively, showing their accordance with the linear response theory.

Keywords: nanoparticles, ferrofluid, magnetic hyperthermia, functionalization

PACS: 05.70.–a, 47.65.Cb, 47.65.Cb, 87.85.jj **DOI:** 10.1088/1674-1056/aba2dc

1. Introduction

In the last decades, the synthesis of iron oxide magnetic nanoparticles (MNPs) has gained much attention,[1,2] because of their applications in the biomedical area, and particularly magnetic imaging[3,4] and hyperthermia therapy trials[5,6] have been studied. In this scope, the magnetite (Fe_3O_4) and maghemite (γ-Fe_2O_3) are the most frequently used MNPs due to their strong magnetic properties, low cytotoxicity, and chemical stability.[7,8] Nevertheless, in order to carry out *in vitro* or *in vivo* experiments using MNPs, it is necessary to suspend them on biological media (*i.e.*, cell culture medium, phosphate buffer saline, isotonic solution, *etc.*) to ensure a reasonable colloidal stability, thereby forming a stable ferrofluid system.[9,10]

Ferrofluids of MNPs with controlled diameters and shapes, are typically produced by using the well-known chemical co-precipitation procedure, where a base solution is added to liquid saline solutions of Fe^{2+}/Fe^{3+}, under an inert environment with adjustable temperature and pH.[11–15] Furthermore, the surface of the MNPs must be coated with functional groups to achieve the anchoring of targeting agents and possibly the transport of drugs to cells or tissues.[16,17] For example, ferrofluids with Fe_3O_4 nanoparticles coated with polyacrylic acid have shown a good efficiency for possible cancer therapy applications.[18] In the same way, the use of oleic acid as stabilizing surface-ligand for aqueous dispersion is achievable by the formation of a double-layer of oleic acid on the surface of MNPs. The formation of a single layer will not allow the MNPs to be dispersed in aqueous solvents, but a large excess of oleic acid used in the synthesis method favors the formation of a double-layer and provides the optimal water dispersibility.[19,20] Double-layer stabilized nanoparticles can be dispersed in polar and non-polar solvents, and this dual lyophilic character allows us to have MNPs highly stable in aqueous solvents.[21,22] In another work, tiny nanoparticles capped with oleic acid ligands have shown an innovative application to industrial catalytic process, due to their high polydispersity.[23]

Superficial modification of the MNPs produces many physical changes, which are exploited to reach a good colloidal stability and diminish the internal dipolar interactions, thus avoiding forming magnetic clusters. Nevertheless, the magnetic properties and monodispersity of the MNPs should not be dramatically modified after this functionalization process. Thus, the main aim of this work is to evaluate the induced changes in the structure and magnetic properties of Fe_3O_4 MNPs which are coated with oleic acid. Later, the power absorption density of the ferrofluid with OAMNP is analyzed

†Corresponding author. E-mail: meduardo2001@hotmail.com

© 2020 Chinese Physical Society and IOP Publishing Ltd

to explore its expected performance in magnetic hyperthermia experiment.

2. Theoretical aspect

The interaction between alternant magnetic field and ferrofluid system can be modeled by using the linear response theory. In this approximation, a linear relationship between the induced magnetization M and H is assumed. Then, the drained power density P on a volume V of ferrofluid is given by Eq. (1).[24] As observed, P depends on its complex magnetic susceptibility χ''_{F}, in addition to the frequency f, H^2, and the magnetic permeability of the empty space $\mu_0 = 4\pi \times 10^{-7}\ \mathrm{N/A^2}$,

$$P = \mu_0 \pi \chi''_{\mathrm{F}} f H^2. \tag{1}$$

When a monodisperse suspended nanomaterial exhibits a superparamagnetic ordering, the susceptibility χ''_{F} can be expressed as a function of its effective relaxation time τ and the equilibrium magnetic susceptibility χ_{F}, obtaining Eq. (2),[24] where, χ_{F} is given by the typical magnetization of Langevin equation $\chi_{\mathrm{F}} = \mu_0 V_{\mathrm{p}} M_{\mathrm{s}}^2 / 3K_{\mathrm{B}}T$, which is satisfied in the linear regime of magnetization $\mu_0 H V_{\mathrm{p}} M_{\mathrm{s}} < k_{\mathrm{B}}T$[25] and sometimes is called the linearity condition. This inequality includes the core volume of an MNP V_{p} and the total saturation magnetization M_{s}.

$$P = \pi \mu_0 \chi_{\mathrm{F}} H^2 \frac{2\pi f \tau}{1 + (2\pi f \tau)^2}. \tag{2}$$

Under the assumption of a polydisperse distribution of suspended nanoparticles, equation (2) must be modified by introducing a distribution function of particle diameters where different magnetic susceptibilities and relaxation times must be taken into account, thus becoming a more complicated expression. Nevertheless, equation (2) also represents an effective mathematical model describing P of a macro-spin array,[25] which possesses an effective diameter, equilibrium susceptibility, and relaxation time.

Regarding the effective relaxation time τ, this parameter takes into account both the Néel relaxation time (τ_{N}) and the Brownian relaxation times (τ_{B}) as expressed in Eq. (3). Thus, τ_{N} includes the effective magnetic anisotropy constant κ_{e} of the suspended MNPs through the Arrhenius law (see Eq. (4)), where τ_0 is the characteristic length of time (typically 1×10^{-9} s). In addition, τ_{B} includes the viscosity η of the liquid medium and the hydrodynamic diameter D_{H} of the MNPs, following the Stokes–Einstein law (Eq. (5))

$$\tau = \frac{\tau_{\mathrm{N}} \tau_{\mathrm{B}}}{\tau_{\mathrm{B}} + \tau_{\mathrm{N}}}, \tag{3}$$

$$\tau_{\mathrm{N}} = \tau_0 \exp\left(\frac{\kappa_{\mathrm{e}} V_{\mathrm{p}}}{K_{\mathrm{B}}T}\right), \tag{4}$$

$$\tau_{\mathrm{B}} = \frac{3\eta}{K_{\mathrm{B}}T} \frac{4\pi}{3} \left(\frac{D_{\mathrm{H}}}{2}\right)^3 = \frac{\pi \eta D_{\mathrm{H}}^3}{2K_{\mathrm{B}}T}. \tag{5}$$

When the energy of a nanomaterial exceeds its anisotropy barrier (by applying H and T) and if the sampling time of the magnetometer is the same as τ_{N} (typically 100 s), the parameter κ_{e} can be approximated by Eq. (6) (Ref. [26]) which involves the blocking temperature $T = T_{\mathrm{B}}$ and a critical core volume V_{p} of the MNPs, and expressed as

$$\kappa_{\mathrm{e}} = \frac{25 T_{\mathrm{B}} K_{\mathrm{B}}}{V_{\mathrm{p}}}. \tag{6}$$

In a physics laboratory, calorimetric trials are typically performed to determine the drained power density on a ferrofluid with density ρ_{F} and specific heat C_{v}.[27,28] For this purpose, equation (7) can be applied. Thus, its specific absorption rate SAR is initially measured and the parameters f and H are programmed to inductively heat the sample. Likewise, the SAR is easily estimated from the heating rate varying with time of the ferrofluid with the help of Eq. (8),[27–29] which includes the fraction of suspended magnetic nanoparticles MNP.

$$P = \rho_{\mathrm{F}} \cdot SAR, \tag{7}$$

$$SAR = \frac{C_{\mathrm{v}}}{m_{\mathrm{np}}} \frac{\mathrm{d}T}{\mathrm{d}t}. \tag{8}$$

3. Materials and methods

3.1. Synthesis and preparation of ferrofluid

The ferrofluid of uncoated MNPs is prepared following a co-precipitation methodology. First, 30 ml of deionized water (previously deoxygenated with N_2) is deposited in a glass test tube and 15-ml deionized water in another one, both are isolated from the atmosphere to avoid absorbing oxygen. A Schlenk flask is depressurized to 500 mm of Hg within 8 min and then, it is filled with N_2. Afterwards, 0.4867 g of $FeCl_3$ (Sigma Aldrich) is dissolved in the first test tube and 0.417 g of $FeSO_4{\cdot}7H_2O$ (Fermont) in the second tube. Subsequently, both solutions are deposited in the flask. The blend is heated at 30 °C under continuous stirring at 400 rpm. At this point a chronometer is started in order to control the addition sequence of the reactants and heating periods. Right after 5 min, 3 ml of 5-M NH_4OH is added by using a peristaltic pump at a volumetric rate of 1.5 ml/min. After 15 min, a syringe needle is inserted into the septum of the flask. 30 min later, the synthesis is finished. A blackish suspension is obtained, indicating the formation of MNPs. The suspension of MNPs is washed four times with deionized water to eliminate the remaining by-products of the synthesis. Finally, a ferrofluid of MNP dispersed in water is obtained.

In the same sense, the procedure to obtain the ferrofluid of OAMNPs includes the aforementioned steps, followed by the addition of oleic acid. After 10 min, the dispersion is maintained at 80 °C for 10 min, and then, at 90 °C for 10 min. Then, 300 μl of oleic acid (Fluka Analytics, reagent grade) is added into the dispersion and kept stirring for 20 min.

Afterwards, the stirring is stopped, and a colloidal dispersion of OAMNPs is obtained. The excess of oleic acid is eliminated by centrifugation at 1.2×10^4 rpm for 1 h and 10 °C. The supernatant is removed and the OAMNPs are resuspended in deionized water. The centrifugation and resuspension in deionized water steps are repeated four times, and finally, the obtained ferrofluid of OAMNP is dialyzed by using a cellulose membrane (Sigma-Aldrich, MWCO 12 kDa, 1 Da $= 1.66054 \times 10^{-27}$ kg).

3.2. Structural and magnetic characterization of ferrofluid

The core diameter of the MNPs is estimated through x-ray diffraction (XRD) measurements by using a Panalytical Empyrean system and its goniometer covers the angular displacement $5^\circ \leq 2\theta \leq 80^\circ$. Then, $\Delta\theta = 0.02^\circ$ is the programmed angular increment and $t = 30$ s is the sampling time for data acquisition. For this purpose, dried samples with 50 mg of coated and uncoated MNPs are placed on specials glass sample holders for XRD. Additionally, dried samples are analyzed through Fourier transform infrared (FTIR) spectroscopy measurements by using a Thermo Scientific Nicolet iS5 spectrometer in an ATR mode.

The scanning electron microscopy (SEM) measurements are obtained by using an MIRA3 (LMU) device of TESCAN company, with 1 nm of resolution capability. Samples are prepared by diluting 10 μl of ferrofluid with coated and uncoated MNPs in 1 ml of deionized water; subsequently, 10-μl aliquot is placed on a carbon conductive tape (5 mm × 20 mm), which is adhered to the special sample holder for SEM. During the next 35 min, this sample is dried at 45 °C inside an oven and then they are covered via gold sputtering.

In order to analyze the colloidal stability of water suspended coated and uncoated MNPs, Zeta potentials are determined at different pH values by means of a Zetasizer SZ90 (Malvern) through using polystyrene folded capillary disposable cells. First, a 0.01-M NaCl solution is prepared with deionized water, then, 100 μl of MNP at 15 mg/ml is added into 10 ml of NaCl solution. Afterwards, the pH of the dilutions is adjusted to a desired value by adding NaOH or HCl. Dispersions with pH values ranging from 2 to 11 are measured three times to determine the mean values and standard deviation. Additionally, the corresponding Z-average hydrodynamic diameter (D_{H}) and polydispersity index (PDI) are measured by using polystyrene disposable cuvettes (10-mm path length, four clear sides).

To determine the fraction of oleic acid covering the surface of the MNPs, thermo-gravimetric (TGA) measurements are realized with the help of a high-resolution Cahn Versa Therm Analyzer and two sample containers with 1.5-g capacity. A container is filled with 60 mg of dried coated MNPs while the second container is filled with the same mass of uncoated MNPs. Then, both samples are separately heated by sweeping the temperature interval 40 °C $< T <$ 850 °C, at 10 °C/min of heating rate. During the experiments, the uncoated MNPs are always heated under an inert N_2-atmosphere (at 25 ml/min of flux) and the coated samples are heated up to 750 °C under N_2-atmosphere, but in the last interval (750 °C $< T <$ 850 °C) the N_2 is replaced by oxygen.

The magnetization loops (at room temperature 300 K) of the MNPs are obtained using a VersaLab vibrating sample magnetometer (VSM) of quantum design. Hence, 5 mg of dried coated and uncoated MNPs are placed into diamagnetic containers and uniform magnetic fields from −30 kOe–30 kOe (1 Oe = 79.5775 A/m) are applied. Magnetization traces following the ZFC–FC protocol are registered establishing $H = 100$ Oe, while the temperature covers the interval 50 K $< T <$ 400 K.

To determine the power absorption density of the OAMNP ferrofluid, a previously reported induction heater is used.[27,28] The system is an alternating magnetic field generator equipped with a fluoroptic thermometer, which is used to determine the ferrofluid heating. This generator is suitable for modifying the applied frequency covering the interval 185 kHz $< f <$ 530 kHz and the amplitude H can be increased up to 35 mT. Three Eppendorf tubes, each with 2 ml of capacity and 1 ml of ferrofluid (at 1 mg/ml each) are prepared. The procedure to obtain the P of each sample begins by placing them one at the time inside an adiabatic cavity in the inner space of the induction coil where the magnetic field is exactly uniform. Hence, while a sample is irradiated by fixing f and H, its temperature is registered and stored using the thermometer connected to a PC. Later, the temperature slope is analyzed offline to estimate the SAR by applying Eq. (8), which is substituted into Eq. (7) to determine the corresponding P. Following a systematic increasing of f and H, the respective dependence P *versus* f and P *versus* H can be determined. In this work, the mean values of P are plotted using the measurements of the three samples including their corresponding standard deviations.

4. Results

The typical XRD spectra obtained from uncoated (dark line) and OAMNP (gray line) samples are displayed in Fig. 1(a), and both measurements show the characteristic peaks of the magnetite structure. Thus, the Miller indices (2 2 0), (3 1 1), (4 0 0), (4 2 2), (3 3 3), and (4 4 0) are clearly distinguished, which correspond to the respective phases $2\theta = 30.16^\circ$, 35.52°, 43.17°, 53.56°, 57.10°, and 62.70° (JCPDS file, No. 19-0629). Using the Scherrer formula (in radian units) $\sigma = k\lambda(\beta(2\theta)\cos(\theta))^{-1}$, the estimated average crystallite sizes of uncoated σ_{uc} and coated σ_{OAMNP} samples are $\sigma_{\mathrm{uc}} = (13 \pm 1)$ nm and $\sigma_{\mathrm{OAMNP}} = (15 \pm 1)$ nm respectively. For this estimation a shape factor $k = 0.94$ is consid-

ered, the x-ray wavelength is $\lambda = 1.54 \times 10^{-10}$ m, and the determined parameters $\beta(2\theta)$ and θ are obtained from Fig. 1(b), which represent the close-up of the main peaks displayed in Fig. 1(a). In order to determine the standard deviation of σ_{uc} and σ_{OAMNP}, an experiment is performed three times, hence an approximated increase of 13% is observed in the magnetic core of OAMNP, these discrepancies can be attributed to random effects of the preparation processes.

Other spurious uncertainties of the average σ can be intrinsically involved in the Scherrer equation when the sample has a polydispersed diameter below 10 nm and a crystal structure with superficial strain.[30] The strain is important if the synthesis method uses high energy and/or temperatures, but it can be neglected when the preparation is based on chemical reactions or liquid-to-solid phase transitions[31] This last characteristic can explain no larger discrepancies in the sizes reported for several polydispersed nanocomposites from XRD, SEM or TEM.[32–34] Therefore, the SEM micrograph of OAMNP in Fig. 1(c) clearly shows that the clusters possess almost spherical shapes, and that some small clusters. The diameter sizes ($n = 400$) are extracted from a set of SEM images and the distribution is represented in Fig. 1(d). After fitting the data to a normal distribution function, the mean diameter is $\sigma_{OAMNP} = (20 \pm 4)$ nm. Whereas, for uncoated samples the corresponding SEM micrograph of Fig. 1(e) and its plotted distribution of diameters in Fig. 1(f) indicate $\sigma_{uc} = (15.5 \pm 3)$ nm. By comparing the values of σ_{OAMNP} and σ_{uc} from XRD and SEM, the discrepancies of 25% and 16% are respectively evidenced, which are probably related to the polydispersion of the samples omitted in the Scherrer equation. Moreover, 23% is the computed discrepancy through the formula $100(1 - \sigma_{uc}/\sigma_{OAMNP})$, and this difference is mainly related to the oleic acid shell.

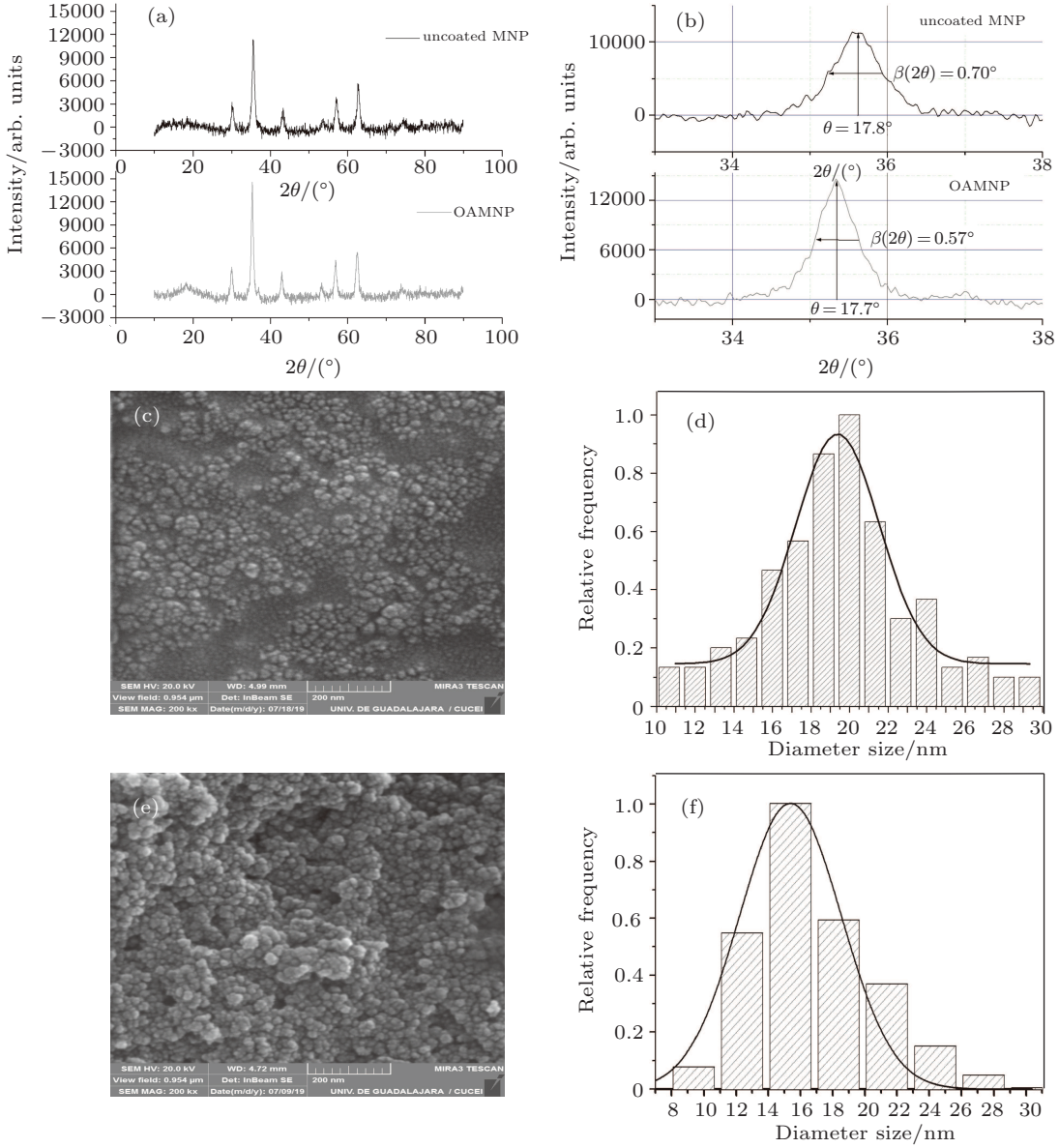


Fig. 1. (a) Typical XRD spectra of uncoated (dark lines) and OAMNP (gray lines) samples, (b) close-up of the main peaks, (c) SEM micrograph of the OAMNP, (d) size distribution plot fitted to a normal data regression, (e) SEM of uncoated MNPs, and (f) corresponding plot including the data regression.

In relation to the superficial modification of the MNPs, the FTIR spectra of pure oleic acid, uncoated and coated MNP are displayed in Fig. 2. In the dark waveform, the presence of Fe_3O_4 is corroborated due to the vibrations observed at 577 cm^{-1} which corresponds to the Fe–O bond, as well as those at 1622 cm^{-1} and 3209 cm^{-1} of the O–H groups.[14] Also, the spectrum of the OA shows its characteristic signals at 3005 cm^{-1} due to the CH stretch at C=CH, 2922 cm^{-1} and 2853 cm^{-1} associated with the asymmetric and anti-symmetric stretch of the CH_2 groups, and an intense signal at 1707 cm^{-1} due to the stretch of the group C=O. The signal observed at 1284 cm^{-1} corresponds to the CO stretch; the signals at 1457 cm^{-1} and 935 cm^{-1} are associated with the OH stretch in the plane and out of the plane respectively; the signal at 722 cm^{-1} corresponds to the CH_2 balance and the signal at 1412 cm^{-1} refers to the vibration of the CH_3 umbrella-like mode of oleic acid.[35] In addition, the spectrum of OAMNP clearly overlaps the last two FTIR spectra and no other structural changes of magnetite are observed. It shows two characteristic signals at 1428 cm^{-1} and 1516 cm^{-1} due to asymmetric and symmetric stretches of the carboxyl group ($–COO^-$) respectively; other signal at 1705 cm^{-1} is due to stretch of group C=O, which corresponds to the characteristic signal of the second layer on the magnetite nanoparticles coated with oleic acid; and finally, the signals at 2847 cm^{-1} and 2915 cm^{-1} are associated with the asymmetric and anti-symmetric stretches of the CH_2 groups, respectively.[14,19] Accordingly, the spectra demonstrate a surface modification of magnetite nanoparticles with an AO double layer coating. Thus, it is expected that the diamagnetic organic coating deposited on MNPs may affect their magnetic properties in comparison with those of uncoated MNPs.

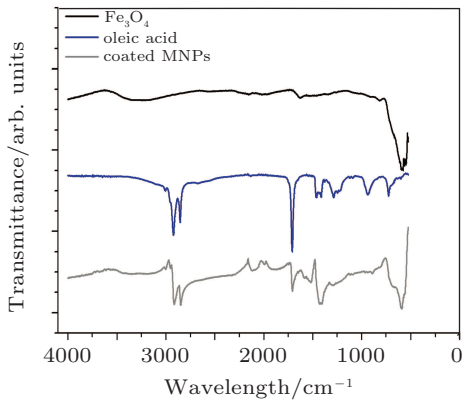


Fig. 2. FTIR spectra of uncoated Fe_3O_4 nanoparticles (dark), pure oleic acid (blue), and OAMNP (gray).

On the other hand, the relative mass dependent temperatures of uncoated (dark line) and OAMNP (gray line) are shown in Fig. 3(a). These measurements are obtained via TGA analysis and two clear different behaviors are observed. After a careful observation of the mass registers, the uncoated MNP sample has 2.87% of mass loss at 39 °C $< T <$ 296 °C and also has 0.45% of mass loss at temperatures above of 296 °C. This decrease is caused by evaporation of water adsorbed on the particle's surfaces. Nevertheless, the sample of OAMNP decreases by 4.4% at 30 °C $< T <$ 165 °C, followed by a 54.4-% mass loss at 165 °C $< T <$ 337 °C. Also, 6.5 % of mass loss at 338 °C $< T <$ 576 °C is observed, and finally, a 3-% decrease above 577 °C. At the end, 31.7% of iron oxide is reached above 750 °C. In the same sense, the derivative of the relative mass loss is shown in Fig. 3(b), where the characteristic peaks of the mass loss rate are highlighted. Hence, the peak at 77 °C of the OAMNP is associated with the water evaporation (4.4% of mass loss), the peaks at 340 °C and 541 °C are related to the boiling point of the oleic acid (60.9% of mass loss) and the last peak at 758 °C to the oxidation of iron oxide (34.7% of relative mass plus resultant material). With the change of atmosphere at $T >$ 750 °C, clearly can be corroborated the expected phase transition from magnetite to hematite.[36] By analyzing the ratio of relative mass proportions between oleic acid and magnetite, 4 nm is the estimated coating thickness. Thus, 19.0 nm is the total diameter of OAMNP which matches the mean value obtained from SEM in Fig. 1(d).

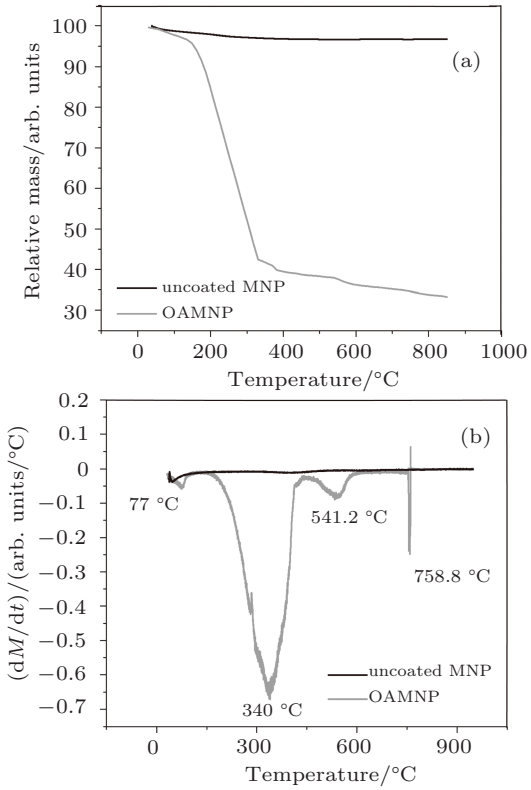


Fig. 3. (a) Relative mass *M versus* temperature of OAMNP over the interval 30 °C $< T <$ 850 °C and (b) corresponding derivative in the same temperature interval.

The measurements of Zeta potential over the pH interval

$2.2 < \mathrm{pH} < 11$ are displayed in Fig. 4(a). For OAMNP, an initial negative decrease of the Zeta potential is observed to reach a minimum value (-80 mV) at $\mathrm{pH} = 8$; this value increases with the systematic increase of pH and it is maintained below -45 mV for $9 < \mathrm{pH} < 11$. Thus, for $\mathrm{pH} > 4$ a good colloidal stability of the OAMNP ferrofluid is achieved. In contrast, the ferrofluid with uncoated MNPs shows a low stability behavior for $\mathrm{pH} > 4$, an incipient stability at $6 < \mathrm{pH} < 7$ and a good stability only for $\mathrm{pH} > 9$. Additionally, the dependence of hydrodynamic diameters D_{H} on pH is shown in Fig. 4(b). In general, the higher D_{H} is observed in uncoated MNPs. Indeed, the largest diameter $D_{\mathrm{H_{max}}} = 5720$ nm is registered at $\mathrm{pH} = 8$, but the Zetasizer cannot determine the corresponding D_{H} for $\mathrm{pH} > 8$, even on its higher resolution scale. When the ferrofluid of OAMNP is analyzed the behavior notably changes, because this parameter systematically decreases with the increase of pH, reaching up to 140 nm at $\mathrm{pH} = 11$. The remarkable differences between the σ_{OAMNP} via SEM and the σ_{OAMNP} via D_{H} are explained by the formation of islands of OAMNP in the ferrofluid, which are probably due to electrostatic and Van Der Waals interactions. A similar trend is observed on the PDI, where the higher values are observed in uncoated MNPs (see Fig. 4(c)). Indeed, for uncoated MNPs, the lowest value $\mathrm{PDI_{min}} = 0.6$ is reached at $\mathrm{pH} = 2$, which indicates a completely polydisperse behavior over the studied pH range. For OAMNP, the measured PDI indicates some polydispersity for $\mathrm{pH} > 8$ and $\mathrm{pH} = 6$. Nevertheless, an acceptable monodispersity is observed at $\mathrm{pH} < 6$ and $\mathrm{pH} = 7.4$; indeed, the best stability values are reached for $\mathrm{pH} = 4$ ($\mathrm{PDI} = 0.13 \pm 0.2$) and $\mathrm{pH} = 7.4$ ($\mathrm{PDI} = 0.18 \pm 0.2$).

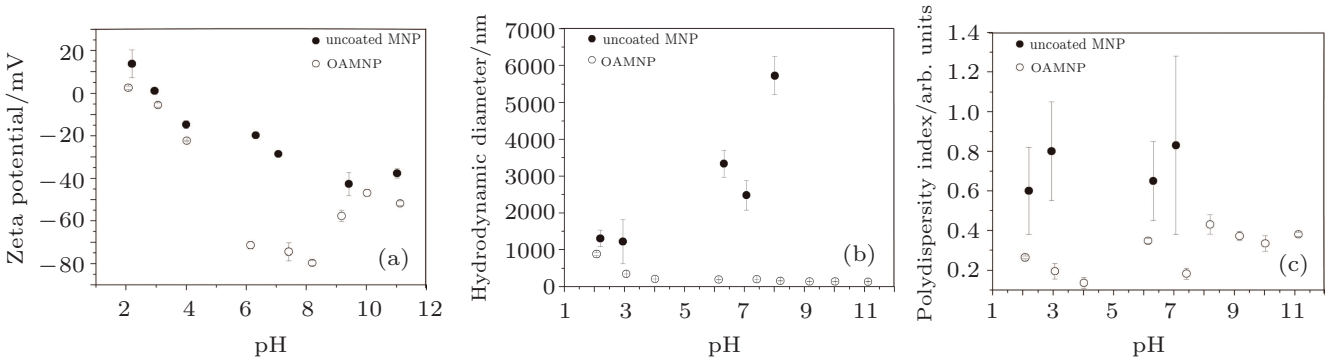


Fig. 4. The pH-dependent (a) Zeta potential, (b) their corresponding hydrodynamic diameters, and (c) polydispersity index of water-suspended coated (open circles) and uncoated (black circles) MNPs.

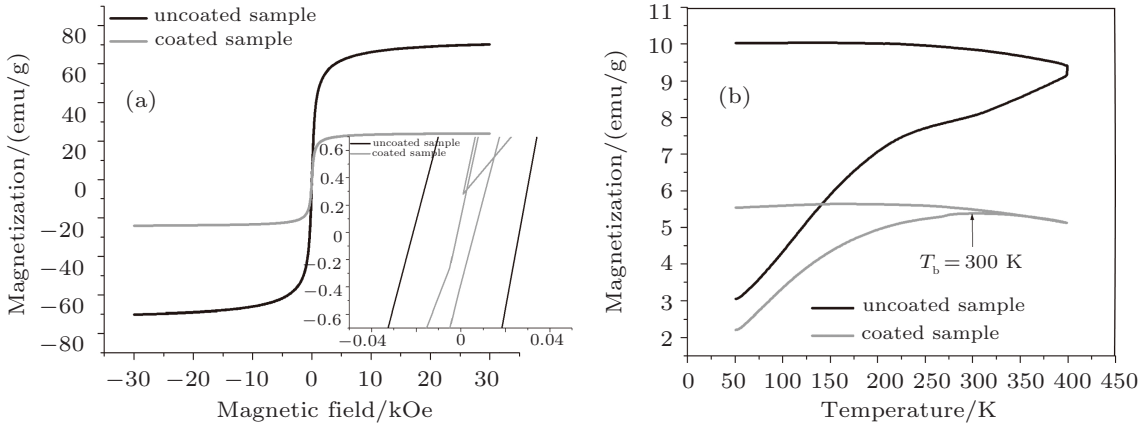


Fig. 5. (a) Magnetization loops at room temperature of uncoated and coated MNPs, and (b) their corresponding ZFC–FC graphs using $H = 100$ Oe.

Magnetic properties of uncoated and coated MNPs under the action of static magnetic field are discussed now. In Fig. 5(a), the curves of magnetization M *versus* magnetic field of the uncoated MNP (dark line) and coated MNP (gray line) are plotted, which are obtained at room temperature. The magnetic saturation of the OAMNP is clearly diminished, reaching $M_{\mathrm{s}} = 24$ emu/g, which is 2.92 times lower than the same parameter obtained for the uncoated sample. Regarding to the magnetic cohercivity H_{c}, a similar result is observed, reaching 11 Oe and 25 Oe for coated and uncoated samples respectively. Also, the low magnetic remanence $M_{\mathrm{r}} = 0.25$ emu/g of OAMNP reaches up to 6.8 times less than the measured in uncoated samples. Hence, those significant differences in the magnetization loop are caused by the lower concentration of magnetite in the OAMNP sample (only 31.7%), in addition, the coating shell helps to diminish the internal dipolar interactions between neighboring particles. Likewise, the dependence of M on temperature following the ZFC–FC protocol

(at $H = 100$ Oe) is shown in Fig. 5(b). Notable differences between both curves can be clearly seen, but the ZFC trace of uncoated samples does not exhibit any maximum value with null slope, indicating the magnetic blocking state of M. Whereas the magnetization of OAMNP exhibits a blocking temperature $T_B = 303$ K, evidencing a superparamagnetic ordering. Despite a low H_c observed on coated samples, the inset of Fig. 5(a) shows some of ferrimagnetic ordering, but the obtained T_B indicates a predominate superparamagnetic behavior above room temperature. These mixed magnetic properties are the consequence of the polydispersity of the samples, which coincides with the measured PDI of Fig. 4(c). Several studies have reported the modulation of T_B as a consequence of a decrease in the dipolar interactions,[37–40] because this potential energy is proportional to r^{-3} and the thickness of the shells increases the distance between nearby magnetic cores. Thus, while the ZFC trace is registered, these weakened interactions do not screen the thermal fluctuations originating from the Néel relaxation of the magnetic moments.

Using the core size σ_{OAMNP} obtained via XRD and the observed blocking temperature T_B, we can obtain $\kappa_e \approx 9.1 \times 10^{-4}$ J/cm^3 from Eq. (6), which is the estimated effective anisotropy constant of OAMNP. In consequence, $\tau_N \approx 88$ s is the effective Néel relaxation time, which is computed by substituting κ_e into Eq. (4). Therefore, the reached Brownian relaxation time $\tau_B \approx 2.7$ ms is computed from Eq. (5) under the assumption of a water viscosity of $\eta = 8.9 \times 10^4$ N·s/m^2 and $D_H \approx 200$ nm. This value is four orders of magnitude less than τ_N, and then $\tau \approx \tau_B$. Thus, the effective relaxation time τ described by Eq. (3) is dominated by the rotation of the OAMNP.

The induced heating on the OAMNP ferrofluid is shown in Fig. 6(a). In this experiment, $H = 25$ mT is the constant amplitude applied during 2 min, while f has been increased in five steps from 182 kHz to 530 kHz. The five traces of the temperature increment over time exhibit an almost linear behavior, where the slope dT/dt systematically grows at each frequency. Indeed, those slopes are computed using data linear regressions in the time interval 20 s $< t <$ 40 s, and also they are used to determine the dependence P *versus* time at each value of f as displayed in Fig. 6(b). Moreover, the parameter P is determined first by computing the corresponding SAR values from Eq. (8), which later is introduced into Eq. (7). For these purposes, are used are the specific heat $C_v = 4.186$ kJ/(K·kg), density $\rho = 1000$ kg/cm^3, and the suspended fraction of OAMNP $m_{np} = 0.1$. The delineated solid line on the plot of Fig. 6(b) is the best linear data fit, which reaches the slope $m_f = 0.047 \pm 0.004$ W/cm^3 per kHz and it is characterized by the quality factor $\chi^2 = 0.94$. This statistical parameter evidences good accordance with P corresponding to the linear response model Eq. (1). Then, $P \approx 22$ W is the maximum power dissipated by OAMNP to 1 cm^3 of water when $H = 25$ mT and $f = 530$ kHz. This magnitude is a very important parameter for future applications in the induction heating of biologic agents.

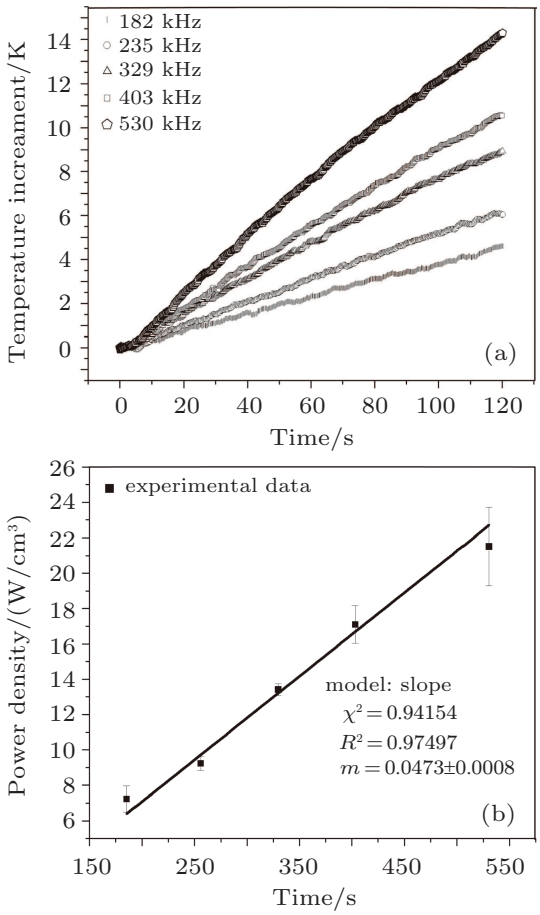


Fig. 6. Time dependent (a) temperature increment during 2 min applying $H = 25$ mT with five values of f, and (b) power density.

In other assays, the OAMNP ferrofluid is heated using the constant frequency $f = 330$ kHz, whereas the amplitude H is increased from 10 mT to 30 mT in steps of 5 mT. In Fig. 7(a), the five traces of the temperature increment during 2 min are shown and the gradual increase of dT/dt with H is evidenced. The same procedure described above (Fig. 6(a)) is used to determine the dependence of P on H and it is displayed in Fig. 7(b). There, the solid line is the best quadratic data fit estimated using the formula $P = m_h \cdot H^2$, where

$$m_h = (0.0237 \pm 0006)\ \text{W/cm}^3\ \text{per}\ (\text{mT})^2$$

is the best computed parameter with quality factor $\chi^2 = 0.99$. Hence, a good concordance between the experimental measurements and the parameter P of Eqs. (1) and (2) can be ensured. In this experiment, $P \approx 21$ W is the maximum power

dissipated by OAMNP to 1 cm^3 of water, when $f = 330$ kHz and $H = 30$ mT.

The linearity condition for P is given by the expression $\mu_0 H V_p M_s < k_B T$, and this inequality can be computed using the employed parameters

$$\mu_0 H = 35 \text{ mT}, \quad V_p = (4/\pi) \cdot 3\,(7.5 \text{ nm})^3,$$
$$T = 315 \text{ K}, \quad M_s = 24 \text{ emu/g};$$

with $M_s = 52.45$ kAm^{-1} converted to MKS units as M (CGS) $= \rho \cdot M$ (MKS). Also, the total density of dried ferrofluid ρ is determined by using the fractions of uncoated magnetite and oleic acid, that is,

$$\rho = 0.609 \cdot \rho_{\text{OleicAcid}} + 0.317 \cdot \rho_{\text{Magnetite}} = 2185.5 \text{ kg/cm}^3,$$

where $\rho_{\text{OleicAcid}} = 895$ kg/cm^3 and $\rho_{\text{Magnetite}} = 5175$ kg/cm^3. Thus, considering the maximum applied amplitude H and the reached maximum temperature, $0.2677 \times 10^{-21} < 4.21 \times 10^{-21}$ is evaluated the inequality of the linear regime condition, which shows concordance with the previous computed quality factor χ^2.

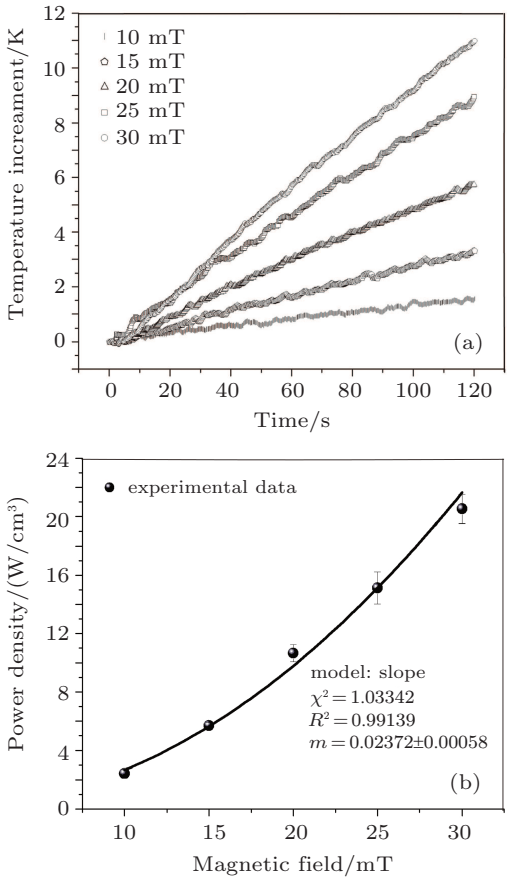


Fig. 7. (a) Temperature increment during 2 min applying $f = 330$ kHz with five steps of H, and (b) the dependence P *versus* H with the corresponding quadratic data regression.

5. Conclusions

In this work, the physical changes of a ferro-colloid system of superficially modified iron oxide MNPs are analyzed. Three principal changes must be highlighted as a consequence of the oleic acid coating, *i.e.* the high colloidal stability related to a low polydispersity index, the modulation of the magnetic properties which leads the magnetization to go up to a superparamagnetic ordering, and the good accordance of its power absorption density with the linear response theory.

Acknowledgement

The authors wish to thank the Mexican institution CONACYT for the scholarship of the undergraduate and graduate students, and also thank Thomas M Trent for reviewing the language of the paper.

References

[1] Gupta A K and Gupta M 2005 *Biomaterials* **26** 3995
[2] Wu W, Wu Z, Yu T, Jiang C and Kim W S 2015 *Science and Technology of Advanced Materials* **16** 023501
[3] Babes L, Denizot B, Tanguy G, Le Jeune J J and Jallet P 1999 *Journal of Colloid and Interface Science* **212** 482
[4] Moore A, Marecos E, Bogdanov A Jr and Weissleder R 2000 *Radiology* **214** 568
[5] Jordan A, Scholz R, Wust P, Fähling H and Felix R 1999 *J. Magn. Magn. Mater.* **201** 413
[6] Jordan A, Scholz R, Wust P, Fähling H, Krause J, Wlodarczyk W, Sander B, Vogl T and Felix R 1997 *International Journal of Hyperthermia* **13** 587
[7] Weissleder R A, Stark D D, Engelstad B L, Bacon B R, Compton C C, White D L, Jacobs P and Lewis J 1989 *American Journal of Roentgenology* **152** 167
[8] Philipse A P, Van Bruggen M P and Pathmamanoharan C 1994 *Langmuir* **10** 92
[9] Shen L, Laibinis P E and Hatton T A 1999 *Langmuir* **15** 447
[10] De Vicente J, Delgado A V, Plaza R C, Durán J D and González-Caballero F 2000 *Langmuir* **16** 7954
[11] Dresco P A, Zaitsev V S, Gambino R J and Chu B 1999 *Langmuir* **15** 1945
[12] Shen L, Qiao Y, Guo Y, Meng S, Yang G, Wu M and Zhao J 2014 *Ceram. Int.* **40** 1519
[13] Filippousi M, Angelakeris M, Katsikini M, Paloura E, Efthimiopoulos I, Wang Y, Zamboulis D and Van Tendeloo G 2014 *J. Phys. Chem. C* **118** 16209
[14] Petcharoen K and Sirivat A 2012 *Mater. Sci. Eng. B* **177** 421
[15] Ahn T, Kim J H, Yang H M, Lee J W and Kim J D 2012 *J. Phys. Chem. C* **116** 6069
[16] Kievit F M, Stephen Z R, Veiseh O, Arami H, Wang T, Lai V P, Park J O, Ellenbogen R G, Disis M L and Zhang M 2012 *ACS Nano* **6** 2591
[17] Shkilnyy A, Munnier E, Hervé K, Soucé M, Benoit R, Cohen-Jonathan S, Limelette P, Saboungi M L, Dubois P and Chourpa I 2010 *J. Phys. Chem. C* **114** 5850
[18] Kolen'ko Y V, Bañbre-Loóez M, Rodríguez-Abreu C, Carbó-Argibay E, Sailsman A, Piñiro-Redondo Y, Cerqueira M F, Petrovykh D Y, Kovnir K, Lebedev O I and Rivas J 2014 *J. Phys. Chem. C* **118** 8691
[19] Soares P I P, Laia C A T, Carvalho A, Pereira L C J, Coutinho J T, Ferreira I M M, Novo C M M and Borges J P 2016 *Appl. Surf. Sci.* **383** 240
[20] Yang K, Peng H, Wen Y and Li N 2010 *Appl. Surf. Sci.* **256** 3093
[21] Maity D and Agrawal D C 2007 *J. Magn. Magn. Mater* **308** 46
[22] Mahdavi M, Ahmad M B, Haron M J, Namvar F, Nadi B, Rahman M Z A and Amin J 2013 *Molecules* **18** 7533
[23] Li Y, Ma F, Su X, Shi L, Pan B, Sun Z and Hou Y 2014 *Industrial & Engineering Chemistry Research* **53** 6718
[24] Rosensweig R E 2002 *J. Magn. Magn. Mater.* **252** 370

[25] Carrey J, Mehdaoui B and Respaud M 2011 *J. Appl. Phys.* **109** 083921
[26] Dearing J A, Bird P M, Dann R J and Benjamin S F 1997 *Geophys. J. Int.* **13** 727
[27] Mazon E E, Villa-Martínez E, Hernández-Sámano A, Córdova-Fraga T, Ibarra-Sánchez J J, Calleja H A, Leyva Cruz J A, Barrera A, Estrada J C, Paz J A and Quintero L H 2017 *Rev. Sci. Instrum.* **88** 084705
[28] Mazon E E, Sámano A H, Calleja H, Quintero L H, Paz J A and Cano M E 2017 *Measurement Science and Technology* **28** 095901
[29] Armitage D W, Le Veen H H and Pethig R 1983 *Phys. Med. Biol.* **28** 31
[30] Ingham B 2015 *Crystallography Reviews* **21** 229
[31] Dorofeev G A, Streletskii A N, Povstugar I V, Protasov A V and Elsukov E P 2012 *Colloid Journal* **74** 675
[32] Zhang L Y, Dou Y H, Zhang L and Gu H C 2007 *Chin. Phys. Lett.* **24** 483
[33] Zheng H, Yang Y, Wen F S, Yi H B, Zhou D and Li F S 2009 *Chin. Phys. Lett.* **26** 017501
[34] Wang Z L, Ma H, Wang F, Li M, Zhang L G and Xu X H 2016 *Chin. Phys. Lett.* **33** 107501
[35] Wu N, Fu L, Su M, Aslam M, Wong K C and Dravid V P 2004 *Nano Lett.* **4** 383
[36] Nor W F, Soh S K, Azmi A A, Yusof M S and Shamsuddin M 2017 *Malaysian Journal of Analytical Sciences* **2** 768
[37] El-Hilo M, Chantrell R W and O'Grady Y K 1998 *J. Appl. Phys.* 5114
[38] Dormann J L, Bessais L and Fiorani D 1988 *J. Phys. C: Solid State Phys.* **21** 2015
[39] Knobel M, Socolovsky L M and Vargas J M 2004 *Rev. Mex. Fís.* **50** 8
[40] Nunes W C, Cebollada F, Knobel M and Zanchet D 2006 *J. Appl. Phys.* **99** 08N705